Control of crystal symmetry breaking with halogen substituted benzylammonium in layered hybrid metal-halide perovskites

Tanja Schmitt, Sean Bourelle, Nathaniel Tye, Giancarlo Soavi, Andrew D Bond, Sascha Feldmann, Boubacar Traoré, Claudine Katan, Jacky Even, Siân Dutton, et al.

Control of crystal symmetry breaking with halogen substituted benzylammonium in layered hybrid metal-halide perovskites

Tanja Schmitt,*[,†,‡] Sean Bourelle,[†,§] Nathaniel Tye,[†, §] Giancarlo Soavi,[§,▽] Andrew D. Bond,[⊥] Sascha Feldmann,[†] Boubacar Traore,[∥] Claudine Katan,[∥] Jacky Even,[○] Siân E. Dutton,[†] and Felix Deschler*[,†,◊]

[†]Cavendish Laboratory, University of Cambridge, JJ Thomson Avenue, Cambridge CB3 0HE, United Kingdom

[§]Cambridge Graphene Centre, University of Cambridge, JJ Thomson Avenue, Cambridge CB3 0FA, United Kingdom

[⊥]Department of Chemistry, University of Cambridge, Lensfield Road, Cambridge CB2 1EW, United Kingdom

[∥]Institut des Sciences Chimiques de Rennes, Université de Rennes 1, 263 Avenue Général Leclerc, F-35700 Rennes, France

[○]Institut FOTON, Université de Rennes 1, 20 Avenue des Buttes de Coësmes, F-35700 Rennes, France

ABSTRACT: Layered hybrid metal-halide perovskites with non-centrosymmetric crystal structure are predicted to show spin-selective band splitting from Rashba effects. Thus, fabrication of metal-halide perovskites with defined crystal symmetry is desired to control the spin-splitting in their electronic states. Here, we report the influence of halogen *para*-substituents on the crystal structure of benzylammonium lead iodide perovskites (4-XC$_6$H$_4$CH$_2$NH$_3$)$_2$PbI$_4$ (X = H, F, Cl, Br). Using X-ray diffraction and second-harmonic generation, we study structure and symmetry of single crystal and thin film samples. We report that introduction of a halogen atom lowers the crystal symmetry such that the chlorine- and bromine-substituted structures are non-centrosymmetric. The differences can be attributed to the nature of the intermolecular interactions between the organic molecules. We calculate electronic band structures and find good control of Rashba splittings. Our results present a facile approach to tailor hybrid layered metal halide perovskites with potential for spintronic and non-linear optical applications.

Introduction

Hybrid metal-halide perovskites with composition ABX_3 are solution-processable semiconductors which have recently produced efficient solar cells and light-emitting diodes.[1-3] Important aspects for the success of these perovskites in optoelectronic applications are their apparent tolerance to defects, which manifests in high luminescence yields,[4-5] sharp absorption onsets[6] and microsecond carrier lifetimes.[7-8] Notably, optical and electronic properties of metal-halide perovskite materials can be controlled by changing their chemical composition and crystal structure.[9] For this, different elements and/or organic components are introduced into the hybrid perovskite crystal by varying the precursor materials. For a fixed B-site metal cation, the bandgap is mainly influenced by the X-site halide. For lead hybrid perovskites, the band gap can be tuned over the visible range by the halide composition.[10-11] By increasing the size of the organic molecule on the A-site in hybrid perovskites, the crystal lattice evolves to a Ruddlesden-Popper or Dion-Jacobson type structure.[12-14] A range of organic molecules can be incorporated, for example aliphatic amines, aromatic amines or chiral methylbenzylamine compounds.[15-18] While the main structural feature of these materials remains the metal-halide octahedra, their stoichiometry and structure differ from the classical perovskite formula ABX_3, allowing greater chemical engineering. These materials are commonly referred to as 2D hybrid perovskites, since their metal-halide octahedra form layers separated by the organic molecules. In the electronics states, the layered nature of these 2D hybrid perovskites creates strong quantum and dielectric confinements leading to the formation of excitons with binding energies of several hundred meV.[19]

Recent publications have reported large Rashba parameters with significant spin-dependent band splitting in some 2D hybrid perovskites.[20-22] Materials with such Rashba effects are promising for spintronic applications,[23] since charges with opposite spin occupy regions in momentum space with opposite sign, i.e. they show spin-selective transport. The Rashba effect arises in materials with strong spin-orbit coupling due to the presence of a non-centrosymmetric potential in the crystal structure. Thus, the strength of Rashba effects is closely connected to the symmetry of the material under investigation. The identity and conformation of the organic molecule in the 2D hybrid perovskites is likely to have a strong impact on the symmetry of the metal-halide lattice, and consequently, on its internal crystal

fields. However, changing the organic molecule in the hybrid perovskite structure typically requires re-optimisation of the synthesis protocol and exploration of 2D hybrid perovskites with strong Rashba effects has been mostly unguided so far. New approaches to tailor the 2D hybrid perovskite crystal structure through specific variations of the precursor materials would thus pave the way to controlled generation of Rashba effects in 2D hybrid perovskites.

Here, we report that control over crystal symmetry in 2D hybrid perovskites can be achieved by systematic variation of benzylammonium organic molecules with halogen substitution on the aromatic ring. We use X-ray diffraction and non-linear optical experiments to resolve the crystal structure of the synthesised compounds and to identify the detailed symmetry-lowered crystal structures. We find that the loss of the inversion centre largely maintains the linear optical properties of the unsubstituted 2D hybrid perovskites. First principle simulations show that the halogen substitution does not affect strongly the average electronic band structure but induces spin splittings for the chloro- and bromo-substituted compounds at the band gap edges. Our results demonstrate a versatile route for the fabrication of 2D hybrid perovskites for non-linear optical and spintronic applications.

RESULTS AND DISCUSSION

Single crystal synthesis. The 2D hybrid perovskite compounds (4-XC$_6$H$_4$CH$_2$NH$_3$)$_2$PbI$_4$ with X = H, F, Cl, Br, which will be abbreviated with (BzA)$_2$PbI$_4$, (4-FBzA)$_2$PbI$_4$, (4-ClBzA)$_2$PbI$_4$ and (4-BrBzA)$_2$PbI$_4$ in the following, were synthesised using a solution based one pot synthesis technique which was adopted from literature.[12, 24]

First, the aromatic amine was dissolved in aqueous hydriodic acid with hypophosphorous acid as stabiliser. Subsequently, a stoichiometric amount of lead(II) iodide was added and the mixture was stirred at 90 °C for 2 h to obtain a clear solution and a stable temperature. The solution was then cooled to room temperature to induce crystallisation of the desired perovskite compound. We found that a controlled cooling with gradient 1 K h^{-1} is crucial to obtain large, high quality crystals up to 1 cm (Figure 1). All synthesis was performed under ambient conditions.

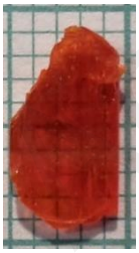

Figure 1. As-synthesised halogen substituted aromatic metal-halide perovskite crystal on millimetre paper. The shown (4-FBzA)$_2$PbI$_4$ crystal is approximately 1 x 0.5 x 0.1 cm.

Halogen effect on crystal structure. We used single crystal X-ray diffraction to analyse the crystal structures of the synthesised *para*-substituted benzylammonium lead iodide perovskites. The structures were determined at 180 K and 300 K and we observed no differences except for a small thermal expansion. All of the compounds adopt a layered structure consisting of an inorganic layer with corner sharing PbI$_6$ octahedra and an organic layer composed of the substituted benzylammonium cations. The parent benzylammonium compound (BzA)$_2$PbI$_4$ adopts the orthorhombic space group *Pbca* which is centrosymmetric and in agreement with earlier work.[16, 25] Introducing fluorine at the *para*-position reduces the symmetry to the monoclinic space group $P2_{1/n}$, but the structure of (4-FBzA)$_2$PbI$_4$ remains centrosymmetric. Introducing the heavier halogens chlorine and bromine at the *para*-position, however, further lowers the symmetry leading to the non-centrosymmetric monoclinic space group $P2_1$ in both (4-ClBzA)$_2$PbI$_4$ and (4-BrBzA)$_2$PbI$_4$ (full structural information and CIF files provided in Supporting Information). The changes in centrosymmetry of the crystal structures are summarised in Table 1.

A detailed analysis of the crystal structures shows that in all four structures, the $[PbI_4]^{2-}$ layers in isolation conform to the layer group $P\ 1\ 2_{1/a}\ 1$, with the Pb atoms occupying inversion centres. These local symmetry elements are present in all $[PbI_4]^{2-}$ layers but they are not always retained as symmetry elements in the 3D space group. The principal interactions between the organic cations and the $[PbI_4]^{2-}$ layers are N^+-H···I hydrogen bonds, which distort the $[PbI_4]^{2-}$ layers away from a regular corner-sharing octahedral arrangement. The positions of the ammonium groups relative to the $[PbI_4]^{2-}$ layers are about the same in all structures studied. Thus, the changes in crystal symmetry originate from the orientation of the cations within each organic layer.

In the non-substituted (BzA)$_2$PbI$_4$ (Figure 2a), the benzylammonium cations are oriented perpendicular to each other, forming edge to face C-H···π interactions (Table 2). The arrangement between nearest benzylammonium cations across the organic layer is parallel displaced revealing strong offset face-to-face π-π-interactions. The organic layer is not centrosymmetric in itself (its layer group is $P\ 2_1\ a\ b$) but the relative arrangement of the inorganic layers is such that their inversion centres are retained as part of the space group *Pbca*.

In the fluorine substituted compound, the cations in direct contact with each $[PbI_4]^{2-}$ layer exhibit an edge-to-face arrangement effectively identical to that in (BzA)$_2$PbI$_4$ but their orientation across the organic layer is different (Figure 2b). The principal intermolecular interactions are again face-to-face π-π-interactions but in this case with interacting molecules arranged across inversion centres. These inversion centres, as well as those in the $[PbI_4]^{2-}$ layers, are retained in the 3D space group $P2_1/n$. In the broader context of this work, it is interesting that both (BzA)$_2$PbI$_4$ and (4-FBzA)$_2$PbI$_4$ adopt an overall centrosymmetric 3D crystal structure, which arises from either locally centrosymmetric or locally non-centrosymmetric organic layers.

Table 1. Symmetry properties of the halogen substituted benzylammonium hybrid lead iodide perovskites.

Compound	Space group	Centrosymmetry	Normalised relative SHG intensity
(BzA)2PbI4	*Pbca*	yes	4
(4-FBzA)2PbI4	$P2_{1/n}$	yes	1
(4-ClBzA)2PbI4	$P2_1$	no	1461
(4-BrBzA)2PbI4	$P2_1$	no	1242

In the isomorphous structures of $(4\text{-ClBzA})_2PbI_4$ and $(4\text{-BrBzA})_2PbI_4$, the orientation of the cations changes from the parallel and perpendicular arrangements to accommodate Cl/Br-π-interactions[26] (Figure 2c, d and Table 2). This structural difference compared to $(BzA)_2PbI_4$ and $(4\text{-FBzA})_2PbI_4$ can be related to the size and electronegativity of the *para*-substituent.[27-28] The resulting arrangement in the organic layer in $(4\text{-ClBzA})_2PbI_4$ and $(4\text{-BrBzA})_2PbI_4$ conforms to layer group *P* 1 2_1 1, which does not contain inversion centres, and the relative arrangement of the $[PbI_4]^{2-}$ layers is such that their local inversion centres are not retained in the 3D space group. Thus, the structure of the organic layer in both compounds, driven by the nature of the intermolecular interactions between the substituted benzylammonium cations, controls the reduction to overall non-centrosymmetry.

In addition to the overall change in space group symmetry, the different orientations of the substituted benzylammonium cations induce subtle changes in the positions and orientations of the ammonium groups which introduce distortions of the PbI_6 octahedra. The degree of distortion can be quantified by the deviation of the Pb-I bond lengths and Pb-$I_{equatorial}$-Pb/I_{axial}-Pb-I_{axial} angles according to the descriptors given by Du et al.[30] (full details in Supporting Information). In short, $(4\text{-ClBzA})_2PbI_4$ and $(4\text{-BrBzA})_2PbI_4$ show a greater

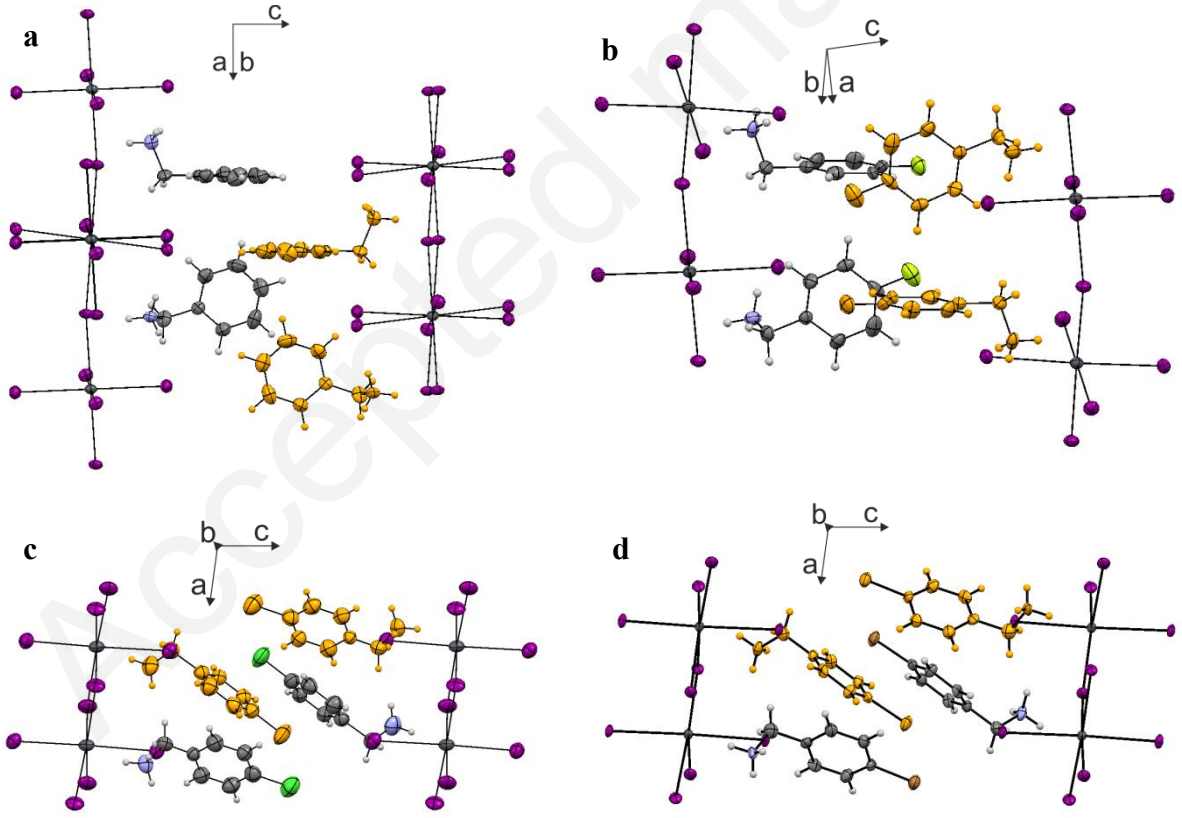

Figure 2. Orientation of the organic cations between the PbI_6 octahedra in (a) $(BzA)_2PbI_4$, (b) $(4\text{-FBzA})_2PbI_4$, (c) $(4\text{-ClBzA})_2PbI_4$ and (d) $(4\text{-BrBzA})_2PbI_4$. The cations in $(BzA)_2PbI_4$ and $(4\text{-FBzA})_2PbI_4$ display perpendicular (edge-to-face) and parallel (face-to-face) arrangements. In contrast, the cations in $(4\text{-ClBzA})_2PbI_4$ and $(4\text{-BrBzA})_2PbI_4$ are tilted on account of π-halogen-interactions.

Table 2. H-π-/X-π-/π-π-distances extracted from crystal structures.

$(BzA)_2PbI_4$		$(4\text{-}FBzA)_2PbI_4$		$(4\text{-}ClBzA)_2PbI_4$		$(4\text{-}BrBzA)_2PbI_4$	
d(H···π)	2.9 Å	d(F···H)	2.4 Å	d(Cl···π)	3.5 Å	d(Br···π)	3.6 Å
$d(\pi\cdots\pi)_{parallel}$	5.0 Å	d(H···π)	2.7 Å	d(Cl···π)	3.7 Å	d(Br···π)	3.8 Å

Extracted distances from XRD shorter or close to the sum of the van der Waals radii indicating strong interactions. Relevant sums of van der Waals radii are $d(H\cdots C_{aromatic})$ = 2.8 Å, $d(F\cdots H_{aromatic})$ = 2.5 Å, $d(Cl\cdots C_{aromatic})$ = 2.8 Å, d(Br···Caromatic) = 3.7 Å.[27] π-π-interactions are reported up to 7.0 Å[29] and Cl/Br-π-interactions up to 4.0 Å[26].

degree of in-plane distortion compared to $(BzA)_2PbI_4$ and $(4\text{-}FBzA)_2PbI_4$.

Non-linear optical properties of the crystal structures. In order to confirm the breaking of the inversion symmetry in the different *para*-substituted benzylammonium crystal structures, we performed optical second-harmonic generation (SHG) experiments. SHG is a non-linear process in which two fundamental photons are converted into one photon with twice the energy. Since SHG can only occur in non-centrosymmetric crystal structures,[31] this technique is ideal to probe the crystal structure of our 2D hybrid perovskite samples. For a centrosymmetric material, the second order susceptibility is equal to zero and no SHG signal from the bulk of the crystal is expected, except for weak SHG from quadrupole scattering and surface effects.[32]

We find that the centrosymmetric compounds $(BzA)_2PbI_4$ and $(4\text{-}FBzA)_2PbI_4$ exhibit only a weak SHG signal, which we attribute to surface effects, while the non-centrosymmetric compounds $(4\text{-}ClBzA)_2PbI_4$ and $(4\text{-}BrBzA)_2PbI_4$ show two orders of magnitude higher SHG intensities (Table 1).

Further, penetration SHG measurements were conducted to distinguish between surface and bulk contributions to the SHG signal. Starting with the detection focus above the crystal surface, we scanned the position of the sample with respect to the beam focus while recording the SHG signal (Figure 3). When hitting the surface of the crystal, a strong and sharp SHG signal is observed for all compounds, which we attribute to a surface effect. Notably, a strong bulk SHG signal is found for the non-centrosymmetric chloro- and bromo-substituted perovskites. The latter SHG signal decays with penetration depth due to absorption of the SHG signal before leaving the sample, so the detected SHG is reduced when the SHG is generated deeper within the sample. These results confirm the non-centrosymmetric crystal structure of the chloro- and bromo-substituted samples, in agreement with the crystal symmetries of the space groups extracted from XRD and the expectations from Neumann's principle, which are that the macroscopic (tensor) properties of a crystal have at least the symmetry of the point group of the space group.[33]

Linear optical properties of the benzylammonium lead iodide compounds. For absorption measurements of $(4\text{-}XBzA)_2PbI_4$ (*X* = H, F, Cl, Br), we fabricate thin films which agree with the single crystal structures in XRD measurements. We observe a sharp peak at the absorption onset, which we attribute to an excitonic transition, as reported previously for 2D hybrid perovskites, followed by a continuum at higher energies which can be attributed to band-band transitions[12, 34] (Supplementary Figure 3). The excitonic peak absorptions of $(4\text{-}XBzA)_2PbI_4$ (*X* = H, F, Cl, Br) are around 2.40 eV, while the band edge energies extracted from Tauc plots are around 2.88 eV (Figure 4a). Both absorption features are slightly blue-shifted by introducing halogen substituents in the series H-F-Br-Cl, which can be attributed to increasing in-plane octahedra distortions.[9, 30]

The exciton binding energies are around 475 meV for all compounds at room temperature. These high binding energies are due to quantum and dielectric confinement and are in good agreement with reported values for similar 2D hybrid perovskites.[19, 34-35]

The external photoluminescence quantum yields are 3 and 2 % for centrosymmetric crystal samples of $(BzA)_2PbI_4$ and $(4\text{-}FBzA)_2PbI_4$, respectively. In contrast, the photoluminescence quantum yields of the non-centrosymmetric crystals of $(4\text{-}ClBzA)_2PbI_4$ and $(4\text{-}BrBzA)_2PbI_4$ are significantly lower with values of about 0.4 % and 0.2 %, respectively. The photoluminescence spectra of $(4\text{-}XBzA)_2PbI_4$ (X = H, F, Cl, Br) consist of multiple features (Figure 4b). The highest energy emission can be attributed to the excitonic emission of 2D hybrid perovskite materials.[19, 30, 34] The excitonic emission peaks are narrow with a slightly asymmetric shape having a tail towards lower energy which may be due to structural disorder.[36] The maxima of the PL intensities are around 2.35 eV/528 nm. The small blue shifts of the PL signals for different halogen substituents are in agreement with the discussed shifts in the absorption spectra.

A further broad, lower energy photoluminescence peak is centred around 1.70 eV/729 nm. Such broad, red-shifted emissions have been observed in layered perovskite materials and may be explained by exciton trapping which produces white light emission, i.e. self-trapping or other trapping mechanisms.[37-42] We find that the excitation power density dependence of the PL from trapped excitons is opposite to the behaviour of the free excitonic emission (Supplementary Figure 5). Upon increasing the excitation power density, the intensity of the broadband red-shifted emission decreases. Thus, a higher excitation density leads to a higher probability to emit from free excitonic states than trapped excitonic states, either due to changes in occupation or emission rates. The detailed mechanism of trapped state emission remains to be fully understood and is beyond the focus of the present study. We note, that the compounds $(4\text{-}XBzA)_2PbI_4$ (*X* = H, F, Cl, Br) presented in this work, are one of the rare examples of lead iodide perovskites

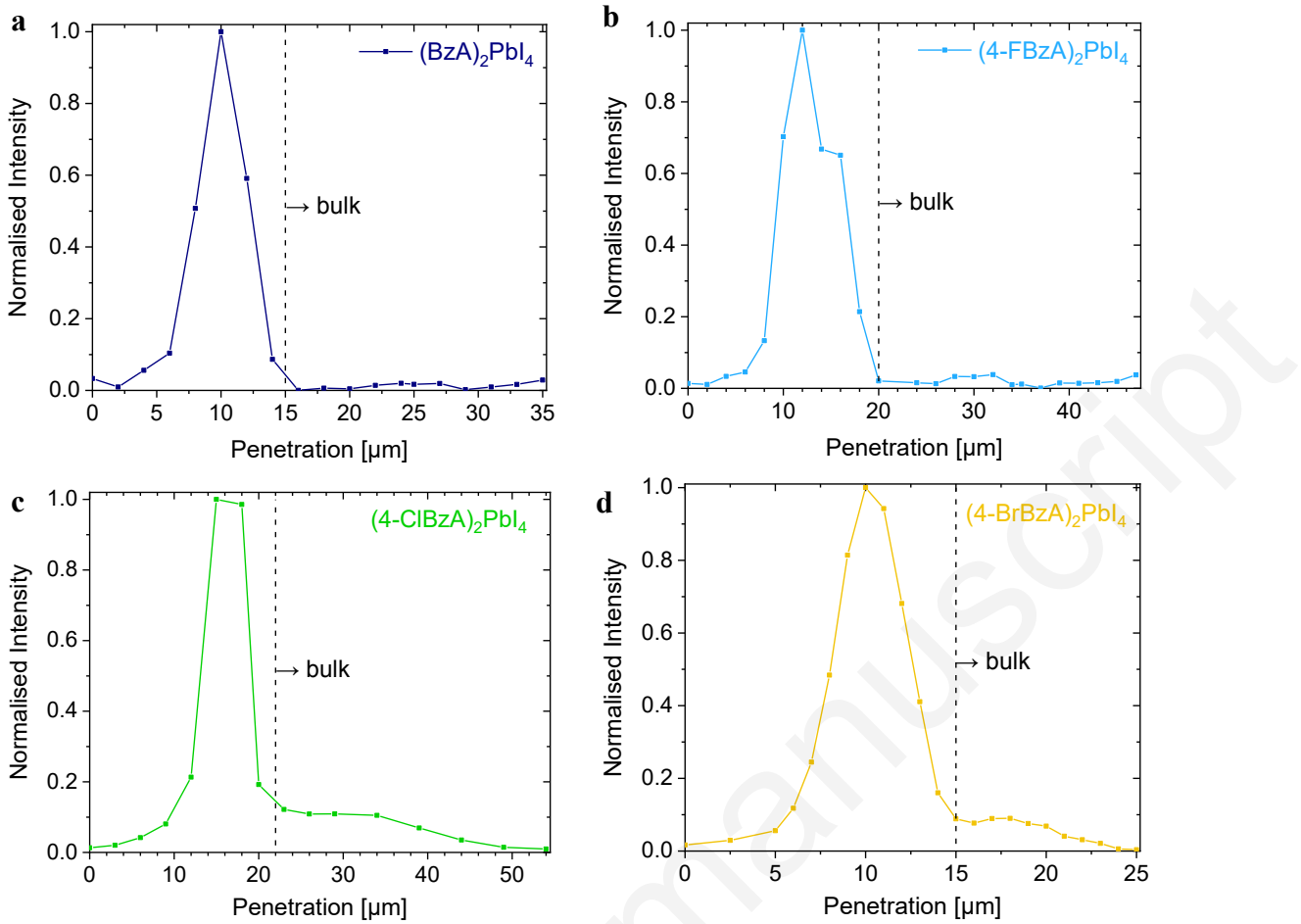

Figure 3. Penetration scans of (4-*X*BzA)$_2$PbI$_4$ (*X* = H, F, Cl, Br). The centrosymmetric crystals of (a**)** (BzA)$_2$PbI$_4$ and (b) (4-FBzA)$_2$PbI$_4$ exhibit only a surface contribution to the SHG signal while for the non-centrosymmetric crystals of (c**)** (4-ClBzA)$_2$PbI$_4$ and (d) (4-BrBzA)$_2$PbI$_4$ an additional bulk contribution to the SHG signal is observed.

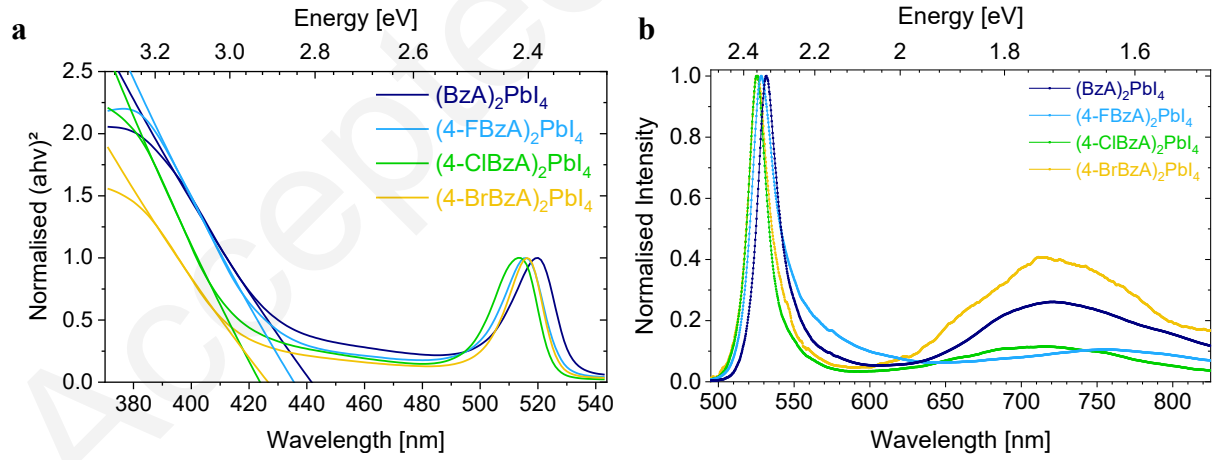

Figure 4. Linear optical propertiesof *para*-substituted benzylammonium lead-halide perovskites. **(a)** Tauc plots were determined from optical transmission experiments of (4-*X*BzA)$_2$PbI$_4$ (*X* = H, F, Cl, Br) thin films according to Lambert-Beer Law with the band edges extracted by linear extrapolation, (b) photoluminescence spectra showing excitonic emission as well as a broad red-shifted emission.

which show white light emission at room temperature[43-45] (Supplementary Figure 4).

Electronic band structure calculations. Electronic band structures of the studied 2D hybrid perovskite compounds were calculated from first-principles Density Functional Theory (DFT). The band structures were calculated for the experimental crystal structures obtained at 180 K and 300 K. Besides a slight modification

of the band gap (< 0.02 eV), electronic properties remains almost unchanged when going from the low to the room temperature structure (Supplementary Figure 6). Calculations of the density of states show that the valence band maximum is a hybridisation between Pb *6s* and I *5p* states with a major contribution from I *5p*. The conduction band minimum is mainly a hybridisation between Pb *6p* states. This holds true for all four compounds (4-*X*BzA)$_2$PbI$_4$ (*X* = H, F, Cl, Br) and agrees with the results for most hybrid lead halide perovskites.[12, 15-16, 46]

The electronic band structures of our studied compounds show highly dispersive states at the band gap (Figure 5a-d). The effective masses are relatively low in the in-plane direction where inorganic octahedra are corner connected, ensuring good in-plane electronic coupling. The calculated band gaps at 300 K are 1.23 eV (*X* = H), 1.24 eV (*X* = F) and 1.26 eV (*X* = Cl, Br). Although band gaps are underestimated with Perdew-Burke-Ernzerhof (PBE) level of theory,[47-48] the trend of increasing band gap with heavier halogen substituent agrees with the experimental data. More significantly, the band gaps of (BzA)$_2$PbI$_4$ and (4-FBzA)$_2$PbI$_4$ are direct while the band gaps of (4-ClBzA)$_2$PbI$_4$ and (4-BrBzA)$_2$PbI$_4$ are indirect due to spin splitting (Figure 5c and d). Corresponding spin textures reveal non-pure Rashba effect[21, 23] (Figure 5e and f). The Rashba splitting is most pronounced for the conduction band

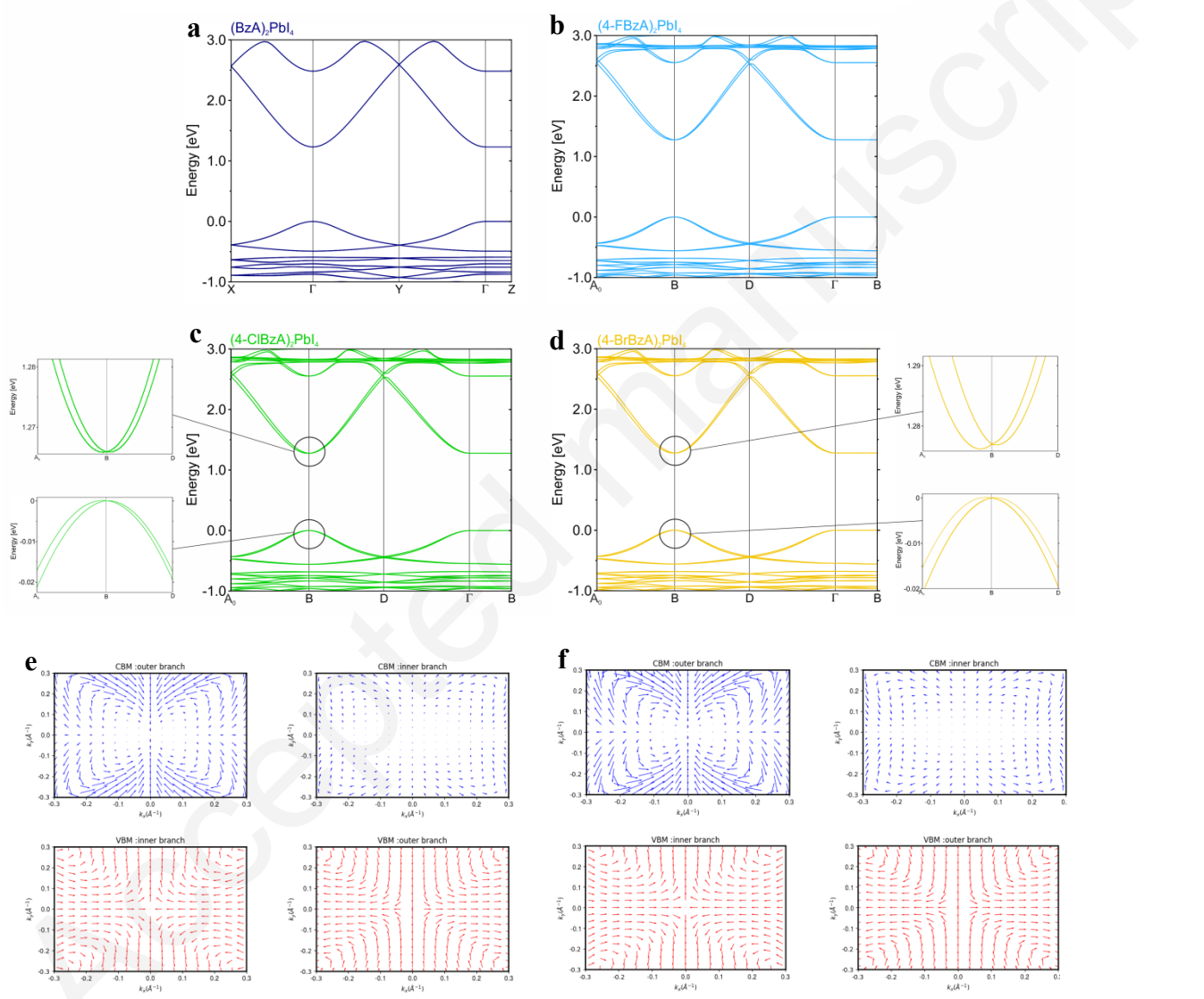

Figure 5. First-principles calculations of electronic band structures of (a) (BzA)$_2$PbI$_4$, (b) (4-FBzA)$_2$PbI$_4$, (c) (4-ClBzA)$_2$PbI$_4$ and (d) (4-BrBzA)$_2$PbI$_4$ at 180 K. For (4-ClBzA)$_2$PbI$_4$ and (4-BrBzA)$_2$PbI$_4$ the spin-split band edges are highlighted by zoom-ins. (e-f) spin textures for the inner and outer branches for valence (red) and conduction (blue) bands of (4-ClBzA)$_2$PbI$_4$ and (4-BrBzA)$_2$PbI$_4$, respectively. The spin textures of both compounds show similar shapes and features, yet with differences in absolute values.

of (4-BrBzA)$_2$PbI$_4$ with a computed Rashba parameter α_R = 2E0/Δk of 260 meV · Å at 180 K. At room temperature, the spin splitting narrows for both non-centrosymmetric compounds. This is likely to be related to thermal expansion which changes octahedral distortion. The calculated splittings are in good agree-

ment with experimental results on similar systems, where values for the Rashba parameter of 500 meV · Å to 1 eV · Å were reported.[20]

CONCLUSIONS

The role of the organic cations in 2D hybrid perovskites is often neglected. We show that *X*-π-interactions in *para*-substituted benzylammonium lead iodide perovskites are crucial for the orientation of the organic cations, which in turn determine the orientation of the PbI_6 octahedra and the overall space group of the crystal structure. In this work, we report that non-centrosymmetry can be designed with *X*-π-interactions. Due to the formation of strong *X*-π-interactions, the symmetry within the $(4\text{-}X\text{BzA})_2PbI_4$ (*X* = H, F, Cl, Br) series lowers with heavier halogen substituents. The isomorphous compounds $(4\text{-ClBzA})_2PbI_4$ and $(4\text{-BrBzA})_2PbI_4$ exhibit a non-centrosymmetric crystal structure and a bulk SHG signal. Combined with band structure calculations and experimentally determined PLQE values, our results demonstrate that control of *X*-π-interactions between organic cations enables design of non-centrosymmetric perovskite materials from initially centrosymmetric structures. This opens a new discovery route for hybrid perovskites with potential for non-linear optical and spintronic applications.

ASSOCIATED CONTENT

Supporting Information.

Synthetic details, sample preparation, experimental and computational details as well as additional figures as described in the text [placeholder for link]
X-ray crystallographic data of benzylammonium lead(II) iodide $(BzA)_2PbI_4$ [placeholder for link]
X-ray crystallographic data of 4-fluorobenzylammonium lead(II) iodide $(4\text{-FBzA})_2PbI_4$ [placeholder for link]
X-ray crystallographic data of 5-chlorobenzylammonium lead(II) iodide $(4\text{-ClBzA})_2PbI_4$ [placeholder for link]
X-ray crystallographic data of 4-bromobenzylammonium lead(II) iodide $(4\text{-BrBzA})_2PbI_4$ [placeholder for link]
This material is available free of charge via the Internet at http://pubs.acs.org.

AUTHOR INFORMATION

Corresponding Author

*Tanja.Schmitt@uni-heidelberg.de
*felix.deschler@wsi.tum.de

Present Addresses

‡Physikalisch-Chemisches Institut, Ruprecht-Karls-Universität Heidelberg, Im Neuenheimer Feld 253, 69120 Heidelberg, Germany
▽Institut für Festkörperphysik, Friedrich-Schiller-Universität Jena, Max-Wien-Platz 1, 07743 Jena, Germany
◊Physik Department, Technische Universität München, Am Coulombwall 4, 85748 Garching, Germany

Author Contributions

T.S. synthesised the materials, took XRD and optical spectroscopy data, and performed data analysis. S.B., N.T. and G.S. took the SHG data. A.B. took the single-crystal XRD data and analysed the crystal structures. S.F. took absorption measurements. B.T., C.K. and J.E. performed first-principles calculations. The manuscript was written by T. S. and F. D. with contributions from all authors.

Notes

The authors declare no competing financial interests.

ACKNOWLEDGMENTS

F.D. acknowledges funding through a Winton Advanced Research Fellowship and the DFG Emmy Noether Program. T.S. acknowledges funding through the ERASMUS program. We thank Ioannis Paradeisanos for his help with the SHG setup. S. B. and N. T. acknowledge funding from EPSRC grant EP/L016087/1. S.F. acknowledges funding from the Studienstiftung des deutschen Volkes and the Engineering and Physical Sciences Research Council (UK). The work at the Institut des Sciences Chimiques de Rennes was supported by Agence Nationale pour la Recherche (TRANSHYPERO project). J.E. acknowledges financial support from the Institute Universitaire de France. This work was granted access to the HPC resources of [TGCC/CINES/IDRIS] under the allocations 2019 A0010907682 made by GENCI.

REFERENCES

1. Bai, S.; Da, P.; Li, C.; Wang, Z.; Yuan, Z.; Fu, F.; Kawecki, M.; Liu, X.; Sakai, N.; Wang, J. T.-W.; Huettner, S.; Buecheler, S.; Fahlman, M.; Gao, F.; Snaith, H. J., Planar perovskite solar cells with long-term stability using ionic liquid additives. *Nature* **2019,** *571* (7764), 245-250.
2. Jung, E. H.; Jeon, N. J.; Park, E. Y.; Moon, C. S.; Shin, T. J.; Yang, T.-Y.; Noh, J. H.; Seo, J., Efficient, stable and scalable perovskite solar cells using poly(3-hexylthiophene). *Nature* **2019,** *567* (7749), 511-515.
3. Xu, W.; Hu, Q.; Bai, S.; Bao, C.; Miao, Y.; Yuan, Z.; Borzda, T.; Barker, A. J.; Tyukalova, E.; Hu, Z.; Kawecki, M.; Wang, H.; Yan, Z.; Liu, X.; Shi, X.; Uvdal, K.; Fahlman, M.; Zhang, W.; Duchamp, M.; Liu, J.-M.; Petrozza, A.; Wang, J.; Liu, L.-M.; Huang, W.; Gao, F., Rational molecular passivation for high-performance perovskite light-emitting diodes. *Nature Photonics* **2019,** *13* (6), 418-424.
4. Deschler, F.; Price, M.; Pathak, S.; Klintberg, L. E.; Jarausch, D.-D.; Higler, R.; Hüttner, S.; Leijtens, T.; Stranks, S. D.; Snaith, H. J.; Atatüre, M.; Phillips, R. T.; Friend, R. H., High Photoluminescence Efficiency and Optically Pumped Lasing in Solution-Processed Mixed Halide Perovskite Semiconductors. *The Journal of Physical Chemistry Letters* **2014,** *5* (8), 1421-1426.
5. Richter, J. M.; Abdi-Jalebi, M.; Sadhanala, A.; Tabachnyk, M.; Rivett, J. P. H.; Pazos-Outón, L. M.; Gödel, K. C.; Price, M.; Deschler, F.; Friend, R. H., Enhancing photoluminescence yields in lead halide perovskites by photon recycling and light out-coupling. *Nature Communications* **2016,** *7*, 13941.
6. De Wolf, S.; Holovsky, J.; Moon, S.-J.; Löper, P.; Niesen, B.; Ledinsky, M.; Haug, F.-J.; Yum, J.-H.; Ballif, C., Organometallic Halide Perovskites: Sharp Optical Absorption Edge and Its Relation to Photovoltaic Performance. *The Journal of Physical Chemistry Letters* **2014,** *5* (6), 1035-1039.
7. deQuilettes, D. W.; Koch, S.; Burke, S.; Paranji, R. K.; Shropshire, A. J.; Ziffer, M. E.; Ginger, D. S., Photoluminescence Lifetimes Exceeding 8 μs and Quantum Yields Exceeding 30% in Hybrid Perovskite Thin Films by Ligand Passivation. *ACS Energy Letters* **2016,** *1* (2), 438-444.

8. Hoye, R. L. Z.; Eyre, L.; Wei, F.; Brivio, F.; Sadhanala, A.; Sun, S.; Li, W.; Zhang, K. H. L.; MacManus-Driscoll, J. L.; Bristowe, P. D.; Friend, R. H.; Cheetham, A. K.; Deschler, F., Fundamental Carrier Lifetime Exceeding 1 μs in Cs2AgBiBr6 Double Perovskite. *Advanced Materials Interfaces* **2018,** *5* (15), 1800464.
9. Knutson, J. L.; Martin, J. D.; Mitzi, D. B., Tuning the Band Gap in Hybrid Tin Iodide Perovskite Semiconductors Using Structural Templating. *Inorganic Chemistry* **2005,** *44* (13), 4699-4705.
10. Sadhanala, A.; Deschler, F.; Thomas, T. H.; Dutton, S. E.; Goedel, K. C.; Hanusch, F. C.; Lai, M. L.; Steiner, U.; Bein, T.; Docampo, P.; Cahen, D.; Friend, R. H., Preparation of Single-Phase Films of CH3NH3Pb(I1–xBrx)3 with Sharp Optical Band Edges. *The Journal of Physical Chemistry Letters* **2014,** *5* (15), 2501-2505.
11. Sadhanala, A.; Ahmad, S.; Zhao, B.; Giesbrecht, N.; Pearce, P. M.; Deschler, F.; Hoye, R. L. Z.; Gödel, K. C.; Bein, T.; Docampo, P.; Dutton, S. E.; De Volder, M. F. L.; Friend, R. H., Blue-Green Color Tunable Solution Processable Organolead Chloride–Bromide Mixed Halide Perovskites for Optoelectronic Applications. *Nano Letters* **2015,** *15* (9), 6095-6101.
12. Stoumpos, C. C.; Cao, D. H.; Clark, D. J.; Young, J.; Rondinelli, J. M.; Jang, J. I.; Hupp, J. T.; Kanatzidis, M. G., Ruddlesden–Popper Hybrid Lead Iodide Perovskite 2D Homologous Semiconductors. *Chemistry of Materials* **2016,** *28* (8), 2852-2867.
13. Mao, L.; Ke, W.; Pedesseau, L.; Wu, Y.; Katan, C.; Even, J.; Wasielewski, M. R.; Stoumpos, C. C.; Kanatzidis, M. G., Hybrid Dion–Jacobson 2D Lead Iodide Perovskites. *Journal of the American Chemical Society* **2018,** *140* (10), 3775-3783.
14. Mitzi, D. B.; Feild, C. A.; Harrison, W. T. A.; Guloy, A. M., Conducting tin halides with a layered organic-based perovskite structure. *Nature* **1994,** *369* (6480), 467-469.
15. Li, W.; Wang, Z.; Deschler, F.; Gao, S.; Friend, R. H.; Cheetham, A. K., Chemically diverse and multifunctional hybrid organic–inorganic perovskites. *Nature Reviews Materials* **2017,** *2*, 16099/1-16099/18.
16. Kamminga, M. E.; Fang, H.-H.; Filip, M. R.; Giustino, F.; Baas, J.; Blake, G. R.; Loi, M. A.; Palstra, T. T. M., Confinement Effects in Low-Dimensional Lead Iodide Perovskite Hybrids. *Chemistry of Materials* **2016,** *28* (13), 4554-4562.
17. Barman, S.; Venkataraman, N. V.; Vasudevan, S.; Seshadri, R., Phase Transitions in the Anchored Organic Bilayers of Long-Chain Alkylammonium Lead Iodides (CnH2n+1NH3)2PbI4; n = 12, 16, 18. *The Journal of Physical Chemistry B* **2003,** *107* (8), 1875-1883.
18. Long, G.; Jiang, C.; Sabatini, R.; Yang, Z.; Wei, M.; Quan, L. N.; Liang, Q.; Rasmita, A.; Askerka, M.; Walters, G.; Gong, X.; Xing, J.; Wen, X.; Quintero-Bermudez, R.; Yuan, H.; Xing, G.; Wang, X. R.; Song, D.; Voznyy, O.; Zhang, M.; Hoogland, S.; Gao, W.; Xiong, Q.; Sargent, E. H., Spin control in reduced-dimensional chiral perovskites. *Nature Photonics* **2018,** *12* (9), 528-533.
19. Blancon, J. C.; Stier, A. V.; Tsai, H.; Nie, W.; Stoumpos, C. C.; Traoré, B.; Pedesseau, L.; Kepenekian, M.; Katsutani, F.; Noe, G. T.; Kono, J.; Tretiak, S.; Crooker, S. A.; Katan, C.; Kanatzidis, M. G.; Crochet, J. J.; Even, J.; Mohite, A. D., Scaling law for excitons in 2D perovskite quantum wells. *Nature Communications* **2018,** *9* (1), 2254/1-2254/10.
20. Yin, J.; Maity, P.; Xu, L.; El-Zohry, A. M.; Li, H.; Bakr, O. M.; Brédas, J.-L.; Mohammed, O. F., Layer-Dependent Rashba Band Splitting in 2D Hybrid Perovskites. *Chemistry of Materials* **2018,** *30* (23), 8538-8545.
21. Kepenekian, M.; Even, J., Rashba and Dresselhaus Couplings in Halide Perovskites: Accomplishments and Opportunities for Spintronics and Spin–Orbitronics. *The Journal of Physical Chemistry Letters* **2017,** *8* (14), 3362-3370.
22. Zhai, Y.; Baniya, S.; Zhang, C.; Li, J.; Haney, P.; Sheng, C.-X.; Ehrenfreund, E.; Vardeny, Z. V., Giant Rashba splitting in 2D organic-inorganic halide perovskites measured by transient spectroscopies. *Science Advances* **2017,** *3* (7), 1700704/1-1700704/6.
23. Kepenekian, M.; Robles, R.; Katan, C.; Sapori, D.; Pedesseau, L.; Even, J., Rashba and Dresselhaus Effects in Hybrid Organic–Inorganic Perovskites: From Basics to Devices. *ACS Nano* **2015,** *9* (12), 11557-11567.
24. Papavassiliou, G. C.; Pagona, G.; Mousdis, G. A.; Karousis, N., Enhanced phosphorescence from nanocrystalline/microcrystalline materials based on (CH3NH3)(1-naphthylmethylammonium)2Pb2Cl7 and similar compounds. *Chem. Phys. Lett.* **2013,** *570*, 80-84.
25. Papavassiliou, G. C.; Mousdis, G. A.; Raptopoulou, C. P.; Terzis, A., Preparation and characterization of [C6H5CH2NH3]2PbI4, [C6H5CH2CH2SC(NH2)2]3PbI5 and [C10H7CH2NH3]PbI3 organic-inorganic hybrid compounds. *Z. Naturforsch., B: Chem. Sci.* **1999,** *54* (11), 1405-1409.
26. Imai, Y. N.; Inoue, Y.; Nakanishi, I.; Kitaura, K., Cl–π interactions in protein–ligand complexes. *Protein Science* **2008,** *17* (7), 1129-1137.
27. Bondi, A., van der Waals Volumes and Radii. *The Journal of Physical Chemistry* **1964,** *68* (3), 441-451.
28. Pauling, L., The nature of the chemical bond. IV. The energy of single bonds and the relative electronegativity of atoms. *Journal of the American Chemical Society* **1932,** *54* (9), 3570-3582.
29. Burley, S. K.; Petsko, G. A., Aromatic-aromatic interaction: a mechanism of protein structure stabilization. *Science* **1985,** *229* (4708), 23-28.
30. Du, K.-z.; Tu, Q.; Zhang, X.; Han, Q.; Liu, J.; Zauscher, S.; Mitzi, D. B., Two-Dimensional Lead(II) Halide-Based Hybrid Perovskites Templated by Acene Alkylamines: Crystal Structures, Optical Properties, and Piezoelectricity. *Inorganic Chemistry* **2017,** *56* (15), 9291-9302.
31. Boyd, R. W., *Nonlinear Optics*. Third Edition ed.; Academic Press: Burlington, 2008.
32. Hollis, D. B., Review of hyper-Rayleigh and second-harmonic scattering in minerals and other inorganic solids. *American Mineralogist* **1988**, 701-706.
33. Burns, G.; Glazer, A. M., *Space Groups for Solid State Scientists*. 2 ed.; Academic Press: 1990.
34. Ogawa, T.; Kanemitsu, Y., FRONT MATTER. In *Optical Properties of Low-Dimensional Materials*, WORLD SCIENTIFIC: 1998; pp 288-339.
35. Ma, Z.-Q.; Shao, Y.; Wong, P. K.; Shi, X.; Pan, H., Structural and Electronic Properties of Two-Dimensional Organic–inorganic Halide Perovskites and their Stability against Moisture. *The Journal of Physical Chemistry C* **2018,** *122* (11), 5844-5853.
36. Stoumpos, C. C.; Soe, C. M. M.; Tsai, H.; Nie, W.; Blancon, J.-C.; Cao, D. H.; Liu, F.; Traoré, B.; Katan, C.; Even, J.; Mohite, A. D.; Kanatzidis, M. G., High Members of the 2D Ruddlesden-Popper Halide Perovskites: Synthesis, Optical Properties, and Solar Cells of (CH3(CH2)3NH3)2(CH3NH3)4Pb5I16. *Chem* **2017,** *2* (3), 427-440.

37. Smith, M. D.; Karunadasa, H. I., White-Light Emission from Layered Halide Perovskites. *Accounts of Chemical Research* **2018,** *51* (3), 619-627.
38. Lin, H.; Zhou, C.; Tian, Y.; Siegrist, T.; Ma, B., Low-Dimensional Organometal Halide Perovskites. *ACS Energy Letters* **2018,** *3* (1), 54-62.
39. Thirumal, K.; Chong, W. K.; Xie, W.; Ganguly, R.; Muduli, S. K.; Sherburne, M.; Asta, M.; Mhaisalkar, S.; Sum, T. C.; Soo, H. S.; Mathews, N., Morphology-Independent Stable White-Light Emission from Self-Assembled Two-Dimensional Perovskites Driven by Strong Exciton–Phonon Coupling to the Organic Framework. *Chemistry of Materials* **2017,** *29* (9), 3947-3953.
40. Yangui, A.; Garrot, D.; Lauret, J. S.; Lusson, A.; Bouchez, G.; Deleporte, E.; Pillet, S.; Bendeif, E. E.; Castro, M.; Triki, S.; Abid, Y.; Boukheddaden, K., Optical Investigation of Broadband White-Light Emission in Self-Assembled Organic–Inorganic Perovskite (C6H11NH3)2PbBr4. *The Journal of Physical Chemistry C* **2015,** *119* (41), 23638-23647.
41. Dohner, E. R.; Hoke, E. T.; Karunadasa, H. I., Self-Assembly of Broadband White-Light Emitters. *Journal of the American Chemical Society* **2014,** *136* (5), 1718-1721.
42. Dohner, E. R.; Jaffe, A.; Bradshaw, L. R.; Karunadasa, H. I., Intrinsic White-Light Emission from Layered Hybrid Perovskites. *Journal of the American Chemical Society* **2014,** *136* (38), 13154-13157.
43. Li, X.; Guo, P.; Kepenekian, M.; Hadar, I.; Katan, C.; Even, J.; Stoumpos, C. C.; Schaller, R. D.; Kanatzidis, M. G., Small Cyclic Diammonium Cation Templated (110)-oriented 2D Halide (X = I, Br, Cl) Perovskites with White-light Emission. *Chemistry of Materials* **2019**.
44. Smith, M. D.; Connor, B. A.; Karunadasa, H. I., Tuning the Luminescence of Layered Halide Perovskites. *Chemical Reviews* **2019,** *119* (5), 3104-3139.
45. Mao, L.; Wu, Y.; Stoumpos, C. C.; Traore, B.; Katan, C.; Even, J.; Wasielewski, M. R.; Kanatzidis, M. G., Tunable White-Light Emission in Single-Cation-Templated Three-Layered 2D Perovskites (CH3CH2NH3)4Pb3Br10–xClx. *Journal of the American Chemical Society* **2017,** *139* (34), 11956-11963.
46. Katan, C.; Mercier, N.; Even, J., Quantum and Dielectric Confinement Effects in Lower-Dimensional Hybrid Perovskite Semiconductors. *Chemical Reviews* **2019,** *119* (5), 3140-3192.
47. Perdew, J. P., Density functional theory and the band gap problem. *International Journal of Quantum Chemistry* **1985,** *28* (S19), 497-523.
48. Zhang, Y.; Yang, W., Comment on ``Generalized Gradient Approximation Made Simple''. *Physical Review Letters* **1998,** *80* (4), 890-890.